2006-09-01

Melt Detection in Antarctic Ice Shelves Using Scatterometers and Microwave Radiometers

David G. Long
david_long@byu.edu

Lucas B. Kunz

Original Publication Citation

Kunz, L. B., and D. G. Long. "Melt Detection in Antarctic Ice Shelves using Scatterometers and Microwave Radiometers." Geoscience and Remote Sensing, IEEE Transactions on 44.9 (26): 2461-9

BYU ScholarsArchive Citation

Melt Detection in Antarctic Ice Shelves Using Scatterometers and Microwave Radiometers

Lukas B. Kunz and David G. Long, *Senior Member, IEEE*

***Abstract*—Ku-band dual-polarization radar backscatter measurements from the SeaWinds-on-QuikSCAT scatterometer are used to determine periods of surface freeze and melt in the Antarctic ice shelves. The normalized horizontal-polarization radar backscatter (σ^o) and backscatter polarization ratio are used in maximum-likelihood estimation of the ice state. This method is used to infer the daily ice-surface conditions for 25 study locations located on the Ronne, Ross, Larsen, Amery, Shackleton, and other ice shelves. The temporal and spatial variations of the radar response are observed for various neighborhood sizes surrounding each given location during the study period. Criteria for determining the dates of melt onset and freeze-up for each Austral summer are presented. Validation of the ice-state and melt-onset date estimates is performed by analyzing the corresponding brightness temperature (T_b) measurements from Special Sensor Microwave/Imager (SSM/I) radiometers. QuikSCAT σ^o measurements from 1999 to 2003 are analyzed and found to be effective in determining periods of melt in Antarctic ice sheets at high temporal and spatial resolutions. These estimates can be used in studies of the climatic effects of the seasonal and interannual melting of the Antarctic ice sheets.**

***Index Terms*—Antarctic, ice, ice shelves, melt onset, QuikSCAT, refreeze, SeaWinds, Special Sensor Microwave/Imager (SSM/I).**

I. INTRODUCTION

A SIGNIFICANT number of studies have been conducted using spaceborne passive microwave sensors to detect the surface melt of Arctic sea ice, e.g., [1]–[3], Antarctic ice sheets [4]–[6], and the Greenland ice sheet [7], [8]; however, the use of active microwave sensors in such studies has been limited [9]. Even more limited has been the use of these instruments in detecting surface melt on Antarctic sea ice [10] and on Antarctic ice shelves [11]. Active microwave measurements, particularly from scatterometers, are very useful in determining annual melt-season duration and in observing surface melt pond formation. These measurements are sensitive to changing ice-surface conditions that may indicate the initial signs of shelf retreat. Recently, longer melt-season duration and the presence of surface melt ponds on Antarctic ice shelves have been linked to shelf breakup [12]. Thus, monitoring surface melt conditions is critical to evaluating the stability of Antarctic ice shelves. This paper proposes a method for exploiting the sensitivity of scatterometer measurements to determine the presence of surface melt on Antarctic ice shelves. Performance of the method is compared with passive microwave measurements.

Manuscript received September 26, 2005; revised February 24, 2006.

L. B. Kunz was with the Microwave Earth Remote Sensing Laboratory, Brigham Young University, Provo, UT 84602 USA. He is now with the Raytheon Missile Systems, Tucson, AZ 85706 USA.

D. G. Long is with the Microwave Earth Remote Sensing Laboratory, Brigham Young University, Provo, UT 84602 USA (e-mail: long@ee.byu.edu).

Digital Object Identifier 10.1109/TGRS.2006.874138

A maximum-likelihood (ML) approach is used to classify the daily ice state from active microwave backscatter measurements from the Ku-band (13.6 GHz) SeaWinds scatterometer on QuikSCAT. Yearly maps of melt-onset dates are created, and the total number of days classified as melt is given for each year. It is shown that these ice-state and melt-onset date estimates agree with corresponding estimates from passive microwave data and provide added insight from the higher spatial resolution and increased sensitivity achieved by an active microwave system.

Section II provides background. Section III explains how distributions are calculated for the melt and nonmelt periods. Section IV contains the proposed ML melt detection method. Section V presents the criteria for determining melt-onset and refreeze dates as well as the mapped results, and Section VI compares the ML method results with observations from radiometer measurements. Finally, conclusions are given in Section VII.

II. BACKGROUND

Spaceborne scatterometers are active microwave sensors that observe the normalized radar backscatter σ^o of the Earth's surface. Scatterometers were originally developed and flown to observe near-surface wind over the ocean [13] but are useful in a variety of terrestrial applications [14]. Scatterometer measurements are particularly sensitive to the water content of the illuminated surface. The backscatter signatures observed from snow-covered ice and liquid water are markedly different [15]. Volume scattering is the predominant factor in the radar response of dry snow cover for active microwave sensors. As the amount of liquid water in the snow cover increases, the wet snow causes a decrease in the radar backscatter [16]. These backscatter signatures are of primary interest in this analysis.

Measurements from radiometers are also useful in analyzing the content of liquid water in the snow cover. Radiometers are passive microwave sensors that record brightness temperature measurements. The relative permittivity of wet snow is considerably higher than for dry snow, so absorption is also higher and results in a decrease of volume scattering. This increases the emissivity and causes the brightness temperature of the wet snow to dramatically increase [16]. Several algorithms have been implemented on passive microwave data to map snowmelt-onset dates on Arctic sea ice [9], the Greenland ice sheet [8], and the Antarctic ice sheet [5], [6]. Similar algorithms are used in this paper to validate the melt detection results from the active microwave measurements on Antarctic ice sheets.

The passive Special Sensor Microwave/Imager (SSM/I) records radiometric T_b measurements with seven channels: dual polarization at 19.35, 37.0, and 85.5 GHz and v polarization at 22.235 GHz [17]. Several SSM/I instruments are onboard Defense Meteorological Satellite Program (DMSP) satellites and provide almost complete coverage of the polar regions each day. Only the 19- and 37-GHz channels are used in this analysis. The SSM/I footprint sizes vary from 43×69 km at 19.35 GHz to 28×37 km at 37 GHz.

The SeaWinds-on-QuikSCAT scatterometer instrument has two scanning pencil-beam antennas and measures both the v and h polarization backscatter [18]. The inner beam is h-polarized with an incidence angle of $\sim 46^\circ$, and the outer beam is v-polarized at an incidence angle of $\sim 54^\circ$. Like the SSM/I, the polar orbiting QuikSCAT provides almost complete coverage of the polar regions daily regardless of cloud cover or solar illumination. The QuikSCAT footprint size is approximately 25×36 km.

Melt conditions can vary over the measurement footprint. To help equalize the sensor resolution and minimize spatial variability effects in the analysis, high-resolution images produced using the Scatterometer Image Reconstruction (SIR) algorithm [19], [20] are used. The SIR algorithm combines all passes from a given day to improve the spatial resolution of the data images at the expense of temporal resolution. Backscatter and T_b images are produced with a pixel size of approximately 2.5 km. The effective resolution for QuikSCAT images is estimated to be 8–12 km, whereas the effective resolution of the SSM/I images is estimated to be of the order of 25–30 and 38–45 km for the 19- and 37-GHz channels, respectively. At each study location, 2.5-km SIR image pixels within a specified radius of the location are included in the analysis. Pass-to-pass variations in sensor sampling locations, antenna sidelobes, and spatial variability of the surface may contribute to variability of the pixel values.

We note that melt conditions vary with the local time of day. Inasmuch as the time of day of observations may differ somewhat between the two sensors, sensor time-of-day acquisition may contribute to differences in the sensor responses. The QuikSCAT SIR image data used in this study are available from the NASA Scatterometer Climate Record Pathfinder (SCP) project [14], [21].

III. Ice-State Distribution Estimations

To observe the intra- and intershelf radar response characteristics, 25 locations are selected from each of the major ice shelves (Fig. 1). The yearly and seasonal variations in the statistics of the measured backscatter values for each location are observed. These empirically calculated statistics form the basis of the ML test for ice-state estimation.

The QuikSCAT scatterometer dual-polarization backscatter measurements (σ_H^o and σ_V^o) are very correlated but exhibit different sensitivities to the presence of liquid water. This sensitivity is easily observed from the quasi-polarization ratio (PR) defined by

$$\mathrm{PR} = \sigma_V^o - \sigma_H^o \tag{1}$$

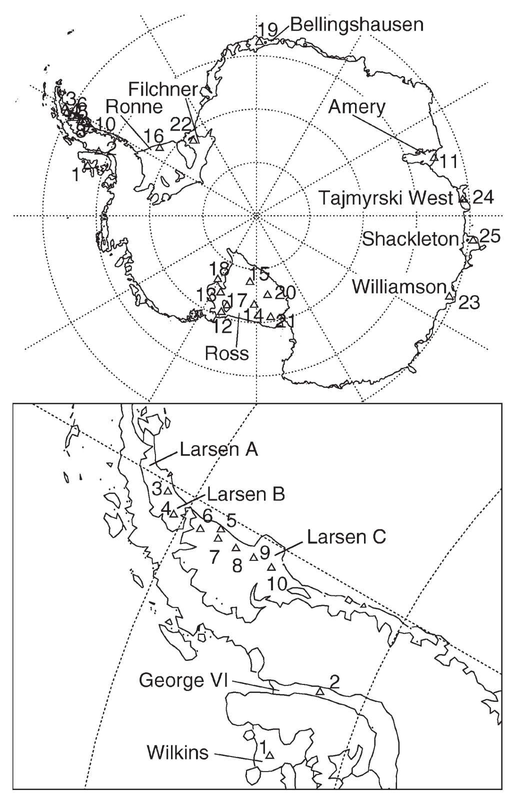

Fig. 1. Twenty-five study locations (top) over Antarctic ice shelves with close-up (bottom) of locations 1–10 on the Antarctic Peninsula. See Table I for latitude and longitude and ice-shelf name of each location.

where the values are in decibels. This is not a true polarization ratio because the v and h polarization measurements are from different incidence angles. In general, σ_V^o is ~ 1 dB below the σ_H^o values.

From the time series in Fig. 2, we see that PR fluctuates much more during each Austral summer than during the winter. This results from the greater sensitivity of h-polarized backscatter to liquid water in the snow cover than v-polarized backscatter as melt/freeze events occur during summer. This time series is typical of most areas that experience surface melting. Backscatter values for locations with no melt events are nearly constant with time.

For each study location, contiguous melt and nonmelt training periods were subjectively selected in the middle of winter and summer of each year, avoiding transition periods. All measurements during the training periods were used to compute melt and nonmelt statistics, which were found not to be particularly sensitive to the precise boundaries chosen.

Fig. 3 shows scatterplots of σ_H^o versus PR for each year of the time series for locations 3 and 7. Note the concentration of nonmelt values around the point (-2 dB, -1 dB) in each plot for location 7. The remaining values, which are during summer melt, are loosely grouped. This suggests that the backscatter and PR observations during melting and nonmelting periods may be modeled as random variables with separate means and covariances for melt and nonmelt. For simplicity, a Gaussian distribution is assumed, and the mean vector and covariance matrix during each specified period in Fig. 2 are computed.

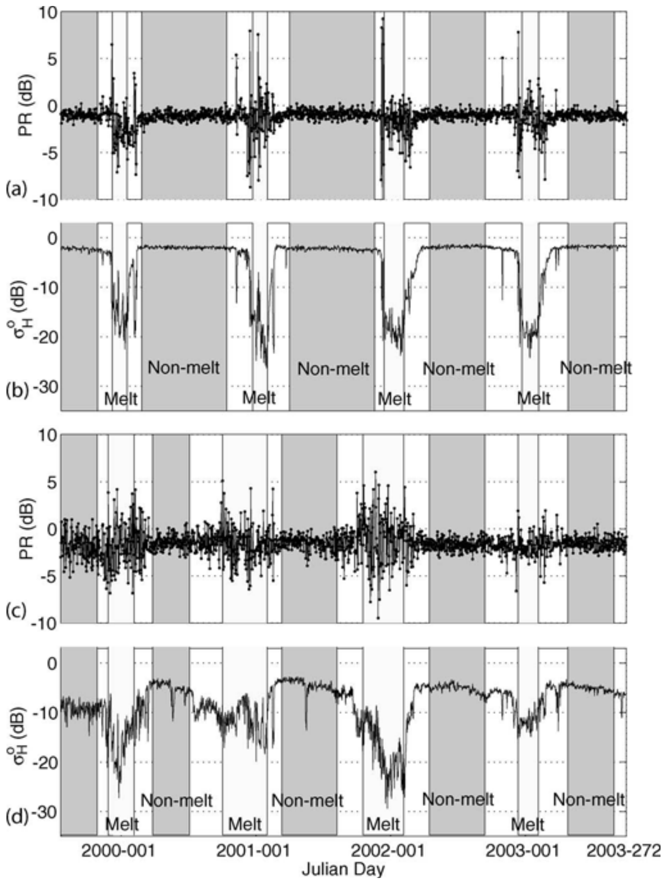

Fig. 2. QuikSCAT time series for study locations 7 and 3 on the Larsen ice shelf. (a) and (c) PR values for locations 7 and 3, respectively. (b) and (d) σ_H^o values for locations 7 and 3, respectively. During each year, contiguous periods (shown as shaded and unshaded boxes) of alternating melt and nonmelt are identified. Each period's mean and covariance are empirically computed and used in ML estimations of the daily ice states. Training regions for melt and nonmelt statistics are indicated. See text for a discussion of location 3.

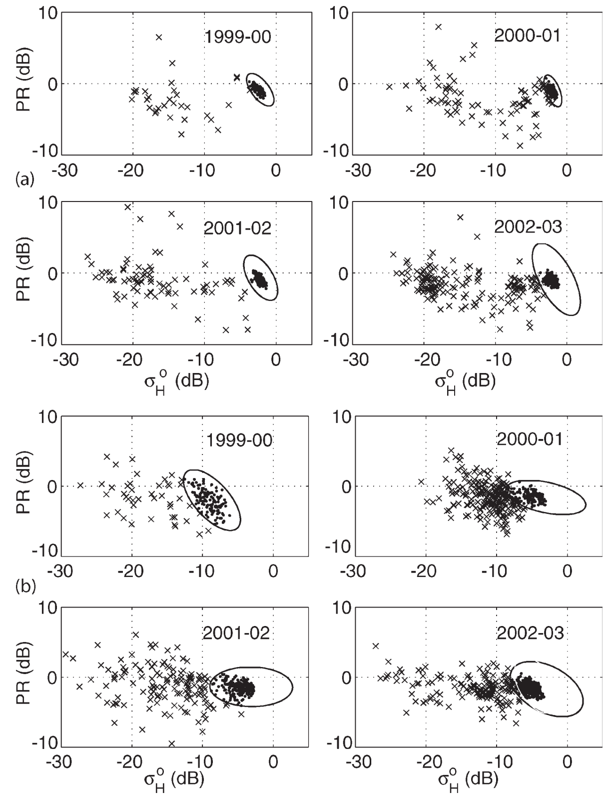

Fig. 3. Yearly backscatter scatterplots for (a) location 7 and (b) location 3. The ellipses are contours of equal Mahalonobis distance from the melt and nonmelt mean values illustrated in Fig. 4. The lighter ellipse corresponds to data values with a 2.25-km (one-pixel) radius, whereas the darker ellipse corresponds to values within a 34-km (15-pixel) radius neighborhood of the location center.

Fig. 4(a) shows the $1-\sigma$ contours of the Gaussian probability density function (pdf) derived for each year's melt and nonmelt periods for all backscatter values collected within a 2.25-km (one-pixel) radius of location 7. These contours describe fairly well the groupings from the scatterplots for location 7 in Fig. 3(a). It is worth noting that the distributions are similar from year to year. To study the spatial consistency of the observations, distributions are also calculated using all values from a neighborhood of radius 34 km around the center of the study location [refer to Fig. 4(b)]. Study locations 1, 2, and 4–10, all located on the Antarctic Peninsula, have very similar nonmelt and melt distributions. These results indicate that the nonmelt and melt distributions are approximately temporally and spatially invariant within a small local area. This property does not extend for locations that may be open water during the summer, e.g., location 3, which is the northernmost study location on the Larsen ice shelf. The time series for this location varies significantly more than for the other peninsular locations due to the summer 2000 breakup of the Larsen "B" ice shelf. In later summers, this location is often open water, which has generally lower, more variable backscatter than ice. Prior to summer 2000, the winter response is from the ice shelf, whereas in later winters, it is from sea ice. In Section VI, the scatterometer observations for this location are shown to be more sensitive to changing shelf-surface conditions than passive microwave observations.

IV. ML Estimation of Ice States

Given the scatterometer measurements, the daily ice state for each location is estimated using the ML ratio method

$$l(\mathbf{x}) = \frac{f_{\mathbf{X}|H_1}(\mathbf{x}|h_1)}{f_{\mathbf{X}|H_0}(\mathbf{x}|h_0)} > \frac{L_{01}P(H_0)}{L_{10}P(H_1)} \tag{2}$$

where $l(\mathbf{x})$ is the ratio of pdfs $f_{\mathbf{x}|H_i}(\mathbf{x}|h_i)$ of $\mathbf{x}$ for each ice state, H_0 denotes the conditions for no surface melting, and H_1 represents the presence of surface melt. $\mathbf{x}$ is a two-element vector in the space spanned by the possible values of σ_H^o and PR, and $\mathbf{m}_0$ and $\mathbf{m}_1$ contain the estimated mean σ_H^o and PR values for the respective ice states. L_{ij} is the loss associated with choosing ice state j when the true state of nature is i, and $P(H_i)$ is the prior probability that ice state i is the true situation. For ML estimation, no *a priori* information is used, and equal losses $(L_{01} = L_{10})$ are chosen.

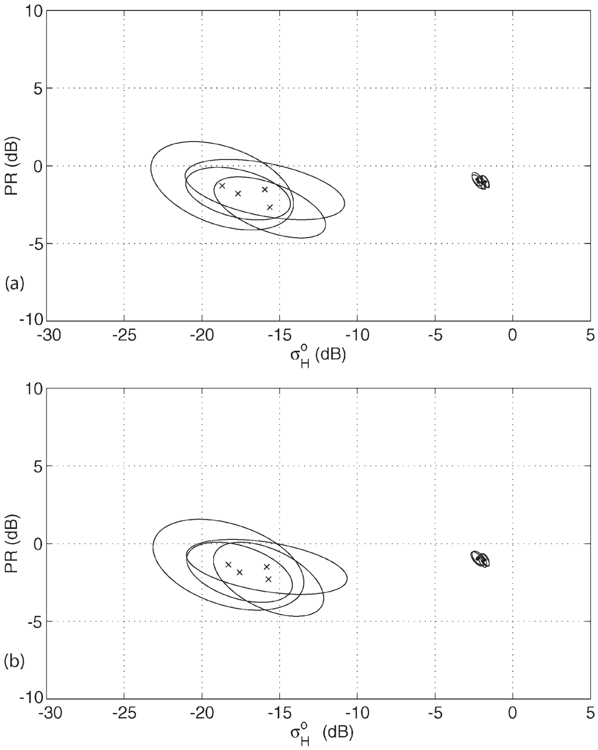

Fig. 4. Yearly bivariate normal distribution $1-\sigma$ covariance contours for data values within (a) a 2.25-km radius (one-pixel radius) neighborhood and (b) a 34-km radius (15-pixel radius) neighborhood of study location 7. The melt period mean for each year is indicated by an $\times$, and each year's nonmelt mean by a dot at the middle of the respective contour. (The distributions for study locations 1, 2, and 4–10 are all similar.)

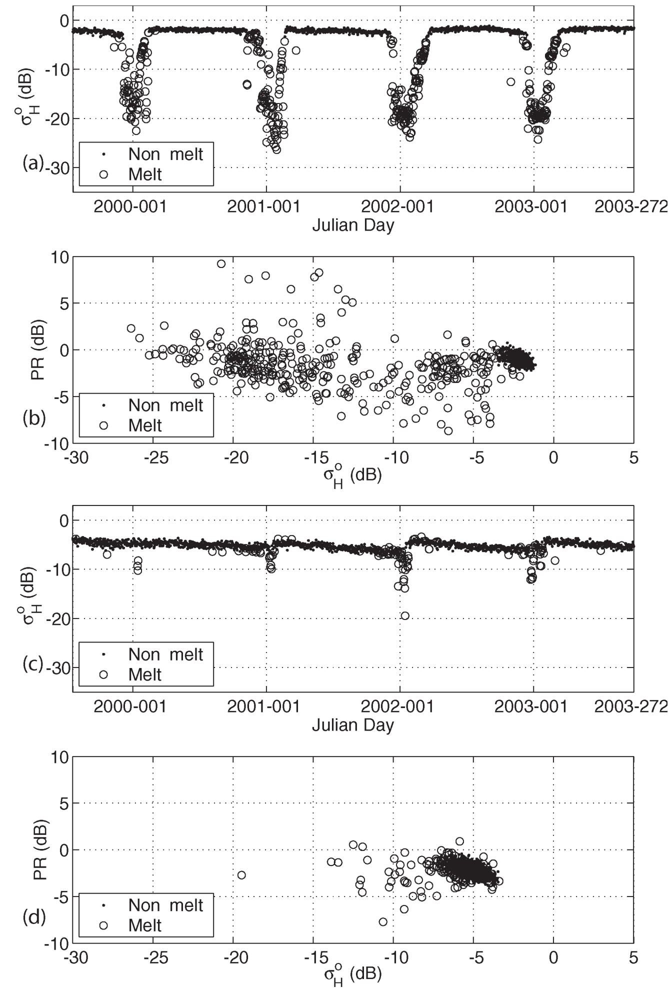

Fig. 5. QuikSCAT backscatter time series and scatterplots for study locations 7 and 19 with resulting ML method surface melt estimates. (a) and (c) Time-series ML estimates for locations 7 and 19, respectively. (b) and (d) Scatterplot ML estimates for locations 7 and 19, respectively. Note the presence of melt classifications for backscatter values higher than the winter mean for location 19 (see text).

Forming the log-likelihood ratio $\Lambda(\mathbf{x}) = \log l(\mathbf{x})$ simplifies the melt hypothesis test to a comparison of weighted norms, the so-called Mahalonobis distance, i.e.,

$$\phi(\mathbf{x}) = \begin{cases} 1, & \|\mathbf{x}-\mathbf{m_1}\|_{\mathbf{R}_1^{-1}} < \|\mathbf{x}-\mathbf{m_0}\|_{\mathbf{R}_0^{-1}} + \log\frac{|\mathbf{R}_0|}{|\mathbf{R}_1|} \\ 0, & \text{otherwise} \end{cases} \quad (3)$$

where $\mathbf{R}_0$ and $\mathbf{R}_1$ are the respective covariance matrices for nonmelt and melt conditions. This test is performed on the daily σ^o values for the 25 study locations from 1999 through 2003. Each day's measurements are used independently in the melt classification, so the result from one day does not influence the ice-state estimation for any other day. The time-series data are divided into yearly segments, and the mean and covariance over each given year are used in the ML test. For locations that exhibit very few days of melting, the empirically computed covariance matrices may be ill conditioned. In these cases, the covariance matrix from the nearest valid location is used instead. This substitution is necessary only for a few locations on the Ronne and Ross ice shelves. Fig. 5 illustrates the results of the ML ice-state estimation for locations 7 and 19. The melt classification results for the other peninsular locations are very similar (see Table I).

This method performs well for location 7 because periods of reduced backscatter are classified as melt. However, due to refreeze events, some days during the summer have high backscatter values that are close to the winter mean value. These are still included in the reported melt duration. These events are observed in the melt classification results for many of the 25 study locations.

Study location 19 shows that some potentially false melt classifications occur when refrozen snow backscatter measurements are higher than the winter nonmelt values [refer to Fig. 5(c)]. This happens when the backscatter values lie to the right of the decision boundary in the σ_H^o versus PR scatterplot [see Fig. 5(d)]. A slight modification to the decision boundary can compensate for this problem; however, because such measurements represent a distinct deviation from the normal nonmelt conditions, the locations classified as melt that have higher backscatter values should be identified and analyzed further. Possible explanations for this behavior include a dramatic refreeze event, the formation of hoar frost, or a significant accumulation event, among others.

Generally, the scatterometer measurements increase dramatically at the end of the Austral summer and indicate the onset of surface refreeze. Some years at the conclusion of the summer melt season, the backscatter measurements rise above the

TABLE I
MELT-ONSET DATES AND TOTAL NUMBER OF MELT DAYS FOR EACH YEAR FROM THE ML QUIKSCAT MELT DETECTION METHOD

Location	Shelf	Longitude	Latitude	1999-00 Onset/Total	2000-01 Onset/Total	2001-02 Onset/Total	2002-03 Onset/Total
1	Wilkins	073.50°W	70.25°S	99-279 / 153	00-306 / 131	01-270 / 103	02-332 / 097
2	George VI	067.90°W	70.90°S	99-311 / 112	00-307 / 070	01-345 / 082	02-332 / 081
3	Larsen B	060.50°W	65.35°S	99-324 / 149	00-257 / 133	01-266 / 159	02-331 / 096
4	Larsen B	061.50°W	65.75°S	99-322 / 099	00-308 / 059	01-334 / 094	02-299 / 078
5	Larsen C	060.91°W	66.95°S	99-337 / 075	00-309 / 089	01-338 / 099	02-341 / 089
6	Larsen C	061.50°W	66.50°S	99-324 / 083	00-308 / 079	01-334 / 099	02-341 / 084
7	Larsen C	061.50°W	67.00°S	99-337 / 075	00-309 / 087	01-338 / 098	02-341 / 091
8	Larsen C	061.50°W	67.50°S	99-337 / 060	00-341 / 078	01-338 / 097	02-341 / 085
9	Larsen C	061.50°W	68.00°S	99-337 / 054	00-341 / 073	01-343 / 091	02-345 / 087
10	Larsen C	061.50°W	68.50°S	99-337 / 054	00-341 / 056	01-343 / 078	02-345 / 083
11	Emery	072.00°E	69.00°S	00-017 / 021	00-334 / 056	01-346 / 055	02-344 / 058
12	Ross	160.00°W	78.50°S	—— / 000	—— / 000	—— / 002	02-365 / 026
13	Ross	155.00°W	80.50°S	—— / 000	—— / 000	—— / 002	—— / 003
14	Ross	178.61°W	79.99°S	—— / 000	—— / 000	—— / 001	—— / 002
15	Ross	174.45°W	82.52°S	—— / 001	—— / 001	—— / 001	—— / 000
16	Ronne	055.00°W	76.75°S	—— / 006	00-362 / 027	01-320 / 018	—— / 016
17	Ross	162.00°W	79.40°S	—— / 000	—— / 000	—— / 001	03-019 / 005
18	Ross	148.77°W	81.66°S	—— / 000	—— / 000	—— / 001	—— / 000
19	Bellingshausen	001.00°E	70.50°S	00-011 / 007	00-306 / 028	01-344 / 050	02-351 / 036
20	Ross	172.00°E	81.00°S	—— / 001	—— / 002	—— / 001	—— / 000
21	Ross	172.00°E	78.50°S	—— / 003	—— / 000	—— / 003	—— / 003
22	Filchner	040.00°W	79.00°S	—— / 018	—— / 018	02-018 / 032	—— / 026
23	Williamson	112.75°E	66.50°S	—— / 000	—— / 000	—— / 000	—— / 000
24	Tajmyrski West	085.50°E	66.75°S	—— / 011	00-333 / 062	01-342 / 063	02-342 / 057
25	Shackleton	096.50°E	65.50°S	99-349 / 041	00-329 / 066	01-331 / 078	02-336 / 094

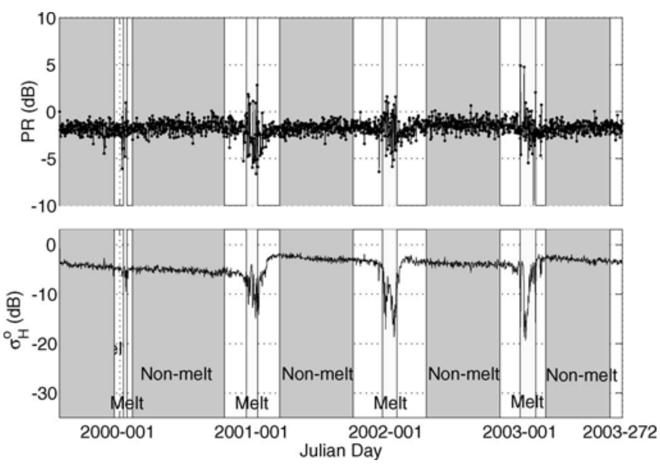

Fig. 6. Time series for study location 24 on the Shackleton ice shelf. The bottom panel of the image shows a significant increase in backscatter following the 2000–2001 melt season that rises ~ 3 dB above the previous winter's mean value. Training regions for melt and nonmelt statistics are indicated.

previous winter's mean value. Study location 24, located on the western Shackleton ice shelf, illustrates this behavior (Fig. 6). The end of the 2000–2001 melt season is marked by σ_H^o values roughly 3 dB above the mean value for the previous winter of 2000. Note that this phenomenon follows a year of significantly more melt than the previous year. Summer melt events lead to the formation of new ice lenses, ice pipes, and other subsurface melt/freeze features, which increase the total backscatter after the freeze. During the winter, snow accumulation buries these melt features and reduces the total backscatter. The slope of the reduction can be used to infer the snow accumulation rate [22].

To validate the ice-state estimates from this ML method, passive microwave observations are also analyzed in Section VI. First, however, the next section discusses mapping the progression of melt onset for the ice shelves.

V. DETERMINING MELT-ONSET AND REFREEZE DATES

As previously noted, the Larsen ice shelf has become the subject of interest for observing and understanding the causes and impacts of ice-shelf breakup. Surface melting is believed to play a key role in ice-shelf breakup [12]. Determining the dates of melt-onset and refreeze is important in understanding the inter-annual variability of surface melt in Antarctica. Previous efforts to map these events have focused on Arctic and Antarctic sea ice. Winebrenner *et al.* [23] used synthetic aperture radar and scatterometer data to map the melt-onset and refreeze dates of Arctic sea ice, and Drinkwater and Liu [10] used scatterometer data to map melt onset of Antarctic sea ice.

Using the ML method for melt detection on Antarctic ice shelves with QuikSCAT data, we adopt the following criteria for determining the melt-onset and refreeze dates. The melt-onset date is chosen to be the beginning of a three-day period of consecutive melt classifications, and the refreeze date is selected as the day marking the start of a period of no melt classifications for at least seven days. Fig. 7 contains maps of the resulting melt-onset date estimates for each year over the Antarctic Peninsula, whereas Fig. 8 maps the total number of days classified as melt events during each Austral summer for the peninsula. For each pixel in the images, the distribution from the nearest study location is used in the ML ice-state classification. Inasmuch as we are interested only in the ice shelves, only locations below 100 m in elevation are used in the melt-onset progression maps shown here.

For the discussion of these melt maps, we follow the terminology used by Vaughan and Doake [24]: the northernmost section of the Larsen ice shelf (just north of study location 3) is termed Larsen "A," the section covered by locations 3 and 4 is Larsen "B," and locations 5–10 span Larsen "C." Location 1 is on the Wilkins ice shelf and location 2 on the George VI ice shelf.

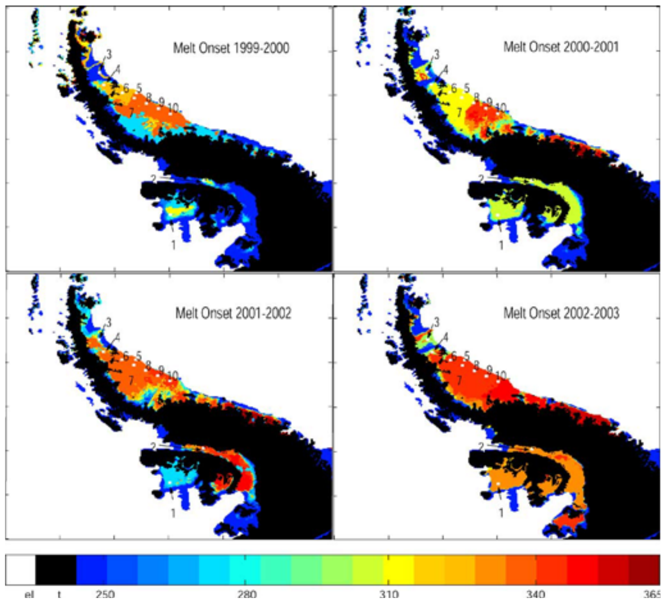

Fig. 7. Melt-onset dates over the Larsen ice shelf for each Austral summer from 1999 to 2003. Melt-onset dates are given as the Julian Day of the year starting the summer, i.e., for the 1999–2000 Austral summer, the melt-onset dates are given as the Julian Day of 1999. The ten study locations in this region are indicated by white dots.

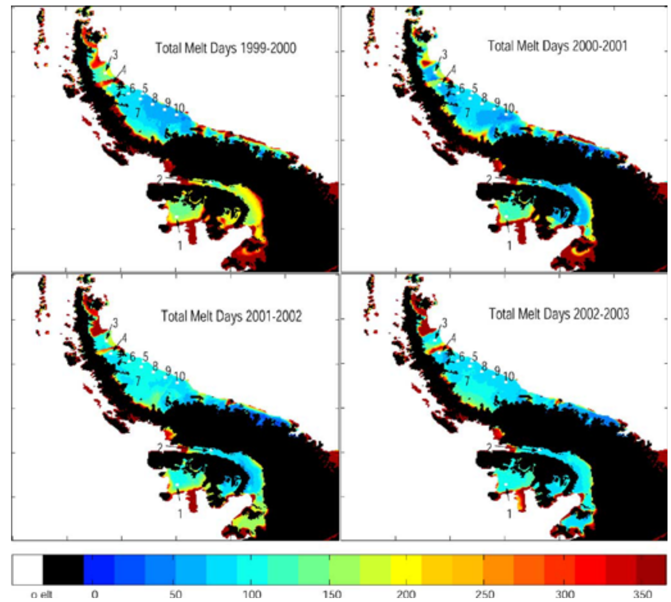

Fig. 8. Total days classified as melt for the Larsen ice shelf during each Austral summer from 1999–2000 to 2002–2003.

From Figs. 7 and 8, we see that the Larsen A ice shelf experiences a very early melt onset and over 300 days of melt each year. From 2001 to 2003, nearly every day is classified as melt. This is expected since Larsen A disintegrated in 1995, thus removing ice-sheet ice from the area [12]. The boundary between the Larsen A and Larsen B ice shelves is marked by an abrupt change in the results from the melt-total and melt-onset maps for each year. The Larsen B melt season begins much later and ends earlier than for Larsen A.

The Larsen C ice shelf experiences significant melt much later than Larsen A and B for the 1999–2000, 2000–2001, and 2002–2003 melt seasons. The total number of melt days for each pixel of Larsen C is almost uniform, but for 2000–2001, the southern portion of the shelf begins its melt season more than a month later than the northern part. The maps also show that although the Larsen C melt season occurs later for 2001–2002 and 2002–2003 than previous summers, the total number of melt days is very similar for each year.

The Wilkins and George VI ice shelves show considerable variation in their respective dates of melt onset from year to year. The 1999–2000 melt season begins earlier on the edges of both shelves than in the interior. This year also experiences a longer melt-season duration than the other years. The 2000–2001 Austral summer is marked by a later melt onset than the previous year, and the melt is uniform over the entire surface of each shelf. During the 2001–2002 and 2002–2003 melt seasons, the total melt on each shelf is very uniform ($\sim$ 100–150 melt days), but the Wilkins shelf begins its melt season nearly three months earlier than the George VI shelf for 2001–2002.

The ML method consistently classifies melt over contiguous areas, and some interesting features are observed in the variations of the melt seasons from year to year. To determine the validity of this melt detection method, an analysis of passive microwave measurements were analyzed using previous methods, and the results are given in the next section.

VI. Validation Using Radiometer Data

Passive microwave brightness temperature measurements have previously been used to detect melt on Arctic sea ice and the Greenland and Antarctic ice sheets from SSM/I observations. The results from three melt detection methods using these data are compared with the ML method classifications using QuikSCAT data.

Anderson [9] used the horizontal range

$$\mathrm{HR} = T_b(19\ \mathrm{H}) - T_b(37\ \mathrm{H}) \tag{4}$$

to determine melting events on Arctic sea ice, where $T_b(19\ \mathrm{H})$ is the h-polarized 19-GHz channel value and $T_b(37\ \mathrm{H})$ is the h-polarized 37-GHz channel value for a given location. If HR drops below 2 K, a melt event is counted. Although this method has previously only been applied to Arctic sea ice, here we use this algorithm with the brightness temperatures of Antarctic shelf ice.

Abdalati and Steffen [7] used the cross-gradient polarization ratio (XPGR) to detect melt over Greenland where

$$\mathrm{XPGR} = \frac{T_b(19\ \mathrm{H}) - T_b(37\ \mathrm{V})}{T_b(19\ \mathrm{H}) + T_b(37\ \mathrm{V})} > -0.0158 \tag{5}$$

is used to classify melt.

A method for determining melt on the Greenland ice sheet proposed by Ashcraft and Long [8] is also implemented using SSM/I 19-GHz v polarization data. This method, hereafter $T_b - \alpha$, uses a threshold set between the mean winter brightness

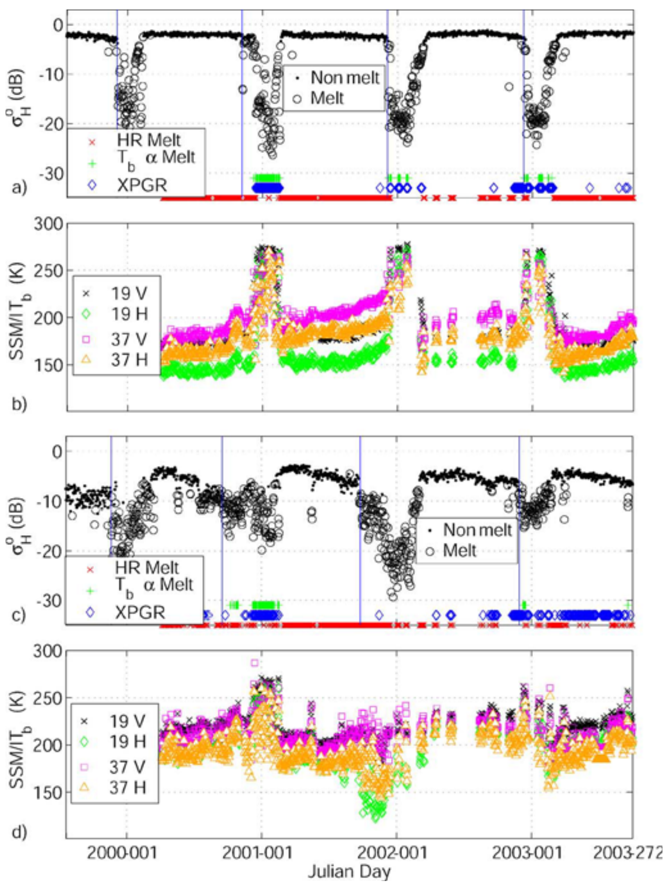

Fig. 9. Melt detection results for study locations 7 and 3 are shown in plots (a) and (c), respectively. ML method melt classifications are indicated on the QuikSCAT time series for each location, whereas the results from the SSM/I methods are given along the bottom of plots (a) and (c) below the QuikSCAT time series. Vertical lines mark the melt-onset dates from the ML method. Plots (b) and (d) contain the SSM/I time series for locations 7 and 3, respectively. ML, $T_b - \alpha$, and XPGR melt classifications are consistent for location 7 but differ for location 3, where $T_b - \alpha$ and XPGR miss the melt season of 2001–2002 and diverge for 2002–2003. The HR method detects melt nearly everyday, and almost no melt during melt periods is detected by the other methods.

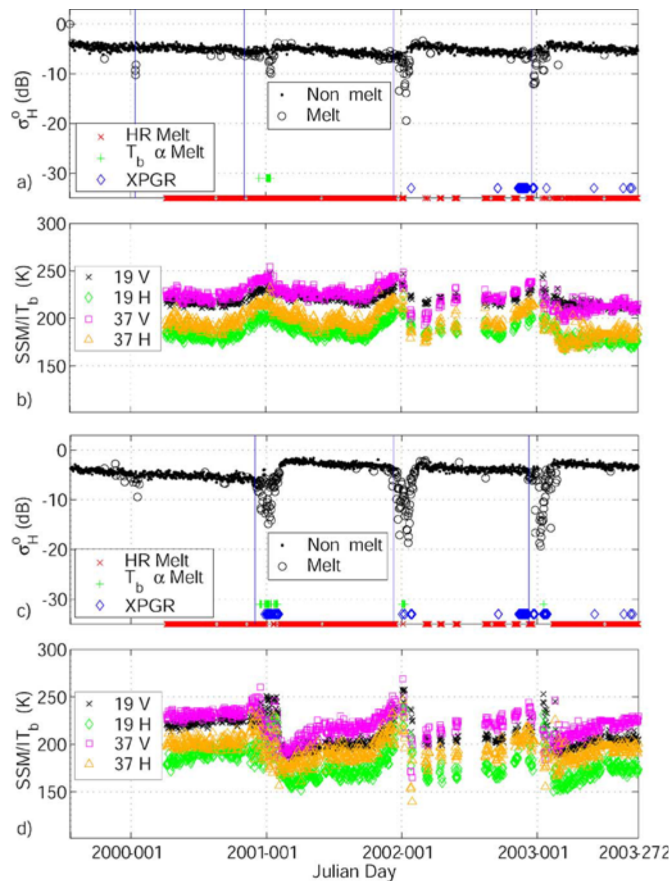

Fig. 10. (a) and (c) Melt detection results for study locations 19 and 24, respectively. (b) and (d) SSM/I time series for locations 19 and 24, respectively. The ML classifies more melt days than the $T_b - \alpha$ and XPGR methods for location 19, and the $T_b - \alpha$ and XPGR results do not coincide for any melt season. For location 24, there is high correlation between the methods except for the 2002–2003 melt season.

temperature value (T_b^{dry}) and the brightness temperature for wet snow (T_b^{wet}). Melt is classified for

$$T_b(19\text{ V}) > \alpha T_b^{\text{dry}} + (1-\alpha) T_b^{\text{wet}} \tag{6}$$

where $T_b^{\text{wet}} = 273$ K and $\alpha = 0.46$ [8].

Figs. 9(b), (d) and 10(b), (d) show the time series of SSM/I data corresponding to the QuikSCAT dataset for four locations. Note that whenever the backscatter decreases significantly, there is usually an accompanying rise in brightness temperature measurements. The data for location 3 in Fig. 9(c) and (d) reveal a deviation from this pattern. The drop in backscatter during the 2001–2002 Austral summer corresponds to varying responses in the T_b values for each SSM/I channel. Inasmuch as passive microwave observations are more subject to changing atmospheric conditions, the discrepancy between the two sensors at this location may be due to atmospheric effects. The variation in responses between the SSM/I channels are due to the different operating frequencies and polarizations. Higher frequency channels are more affected by interference from the atmosphere.

The results of the HR, XPGR, and $T_b - \alpha$ melt algorithms are shown along the bottom of panels (b) and (c) in Figs. 9 and 10. The HR method classifies nearly every day as melt for each of the 25 study locations, whereas the ML, XPGR, and $T_b - \alpha$ results are more consistent. This indicates that the HR method is not portable for use in melt detection on Antarctic ice shelves. The ML method generally results in more days classified as melt than the $T_b - \alpha$ method. XPGR results vary much more from year to year than the other methods as illustrated by the classifications for location 3 [Fig. 9(c)].

The ML method appears to be more sensitive to melt conditions in some cases than the methods using passive microwave data. This is evident in the results for study location 3 in Fig. 9(c). The $T_b - \alpha$ method does not distinguish any melt events during the 2001–2002 summer; however, the backscatter time series clearly indicates substantial melting, and the ML method appropriately identifies many days of surface melt. XPGR sporadically identifies a few days as melt during this period and overestimates the number of melt events for the 2002–2003 summer and winter of 2003.

The total number of melt days and the melt-onset dates from the ML method for the 25 study locations during each year of the study are given in Table I. The melt-onset dates calculated by the ML algorithm are usually a few days prior to the first day of melt detected by XPGR and $T_b - \alpha$. This is the case for the melt season of 2000–2001 for location 7 and for 2000–2001 and 2001–2002 for locations 19 and 24. The XPGR method detects melt prior to the ML method for location 7 during 2001–2002 and 2002–2003 and for locations 3, 19, and 24 during 2002–2003. Melt-onset dates from the ML and $T_b - \alpha$ results are very close during 2001–2002 and 2002–2003 for location 7, during 2000–2001 and 2002–2003 for location 3, and during 2000–2001 for location 24. For most of the study locations, it is observed that when each of the ML, XPGR, and $T_b - \alpha$ methods detect melt during a given melt season, the melt-onset dates for the ML and $T_b - \alpha$ methods are within a few days, whereas the XPGR dates vary considerably.

VII. Conclusion

The ML melt detection algorithm using QuikSCAT Ku-band dual-polarization measurements is shown to be a promising method for detecting surface melt. Melt classifications using this method are spatially consistent, and the melt-onset date estimates correspond to the beginning of periods with greatly reduced backscatter. Maps of the melt-onset progression and melt-season duration for a number of key Antarctic ice shelves were created for each Austral summer from 1999 to 2003.

Validation of the ML method results via passive microwave methods suggests that QuikSCAT measurements are very effective in determining the presence of surface melt on Antarctic ice shelves and that the ML method melt-onset dates and melt-season duration estimates are reliable and consistent. Additionally, the backscatter observed by QuikSCAT is at finer spatial resolution than the radiometer T_b measurements. This allows for more precise observation of spatially varying surface melt. We note, however, that the QuikSCAT time series is significantly shorter than the multidecade SSM/I time series.

Acknowledgment

SeaWinds and QuikSCAT data were obtained from the Physical Oceanography Distributed Data Archive at the Jet Propulsion Laboratory, Pasadena, CA, whereas SSM/I data were obtained from the National Snow and Ice Data Center. This work was completed at the Microwave Earth Remote Sensing Laboratory, Brigham Young University.

References

[1] W. J. Campbell, P. Gloersen, and H. J. Zwally, "Aspects of Arctic sea ice observable by sequential passive-microwave observations from the Nimbus 5 satellite," in *Arctic Technology and Policy*, I. Dyer and C. Chryssostomidis, Eds. New York: Hemisphere, 1984, pp. 197–222.

[2] M. R. Anderson, "The onset of spring melt in first-year ice regions of the Arctic as determined from SMMR data for 1979 and 1980," *J. Geophys. Res.*, vol. 92, no. C12, pp. 13 153–13 163, Nov. 1987.

[3] K. Garrity, "Characterization of snow on floating ice and case studies of brightness temperature change during the onset of melt," in *Microwave Remote Sensing of Sea Ice*, ser. 68, F. Carsey *et al.*, Ed. Washington, DC: Amer. Geophys. Union, 1992, pp. 313–328.

[4] J. Ridley, "Surface melting on Antarctic Peninsula ice shelves detected by passive microwave sensors," *Geophys. Res. Lett.*, vol. 20, no. 23, pp. 2639–2642, Dec. 1993.

[5] H. J. Zwally and S. Fiegles, "Extent and duration of Antarctic surface melting," *J. Glaciol.*, vol. 40, no. 136, pp. 463–476, 1994.

[6] O. Torinesi, M. Fily, and C. Genthon, "Variability and trends of summer melt period of Antarctic ice margins since 1980 from microwave sensors," *J. Clim.*, vol. 16, no. 7, pp. 1047–1060, 2003.

[7] W. Abdalati and K. Steffen, "Greenland ice sheet melt extent: 1979-1999," *J. Geophys. Res.*, vol. 106, no. D24, pp. 33 983–33 988, Dec. 2001.

[8] I. S. Ashcraft and D. G. Long, "Comparison of methods for melt detection over Greenland using active and passive microwave measurements," *Int. J. Remote Sens.*, 2006, to be published.

[9] R. R. Forster, D. G. Long, K. C. Jezek, S. D. Drobot, and M. R. Anderson, "The onset of Arctic sea-ice snowmelt as detected with passive- and active-microwave remote sensing," *Ann. Glaciol.*, vol. 33, pp. 85–93, 2001.

[10] M. R. Drinkwater and X. Liu, "Seasonal to interannual variability in Antarctic sea-ice surface melt," *IEEE Trans. Geosci. Remote Sens.*, vol. 38, no. 4, pp. 1827–1842, Jul. 2000.

[11] H. Rott and K. Sturm, "Active and pssive microwave signatures of Antarctic firn by means of field measurements and satellite data," *Ann. Glaciol.*, vol. 17, pp. 337–343, 1993.

[12] T. A. Scambos, C. Hulbe, M. Fahnestock, and J. Bohlander, "The link between climate warming and break-up of ice shelves in the Antarctic Peninsula," *J. Glaciol.*, vol. 46, no. 154, pp. 516–530, 2000.

[13] F. Naderi, M. Freilich, and D. Long, "Spaceborne radar measurement of wind velocity over the ocean-an overview of the NSCAT scatterometer system," *Proc. IEEE*, vol. 76, no. 6, pp. 850–866, Jun. 1979.

[14] D. Long, M. Drinkwater, B. Holt, S. Saatchi, and C. Bertoia, "Global ice and land climate studies using Scatterometer image data EOS," *Trans. Amer. Geophys. Union*, vol. 82, no. 43, p. 503, Oct. 2001.

[15] F. D. Carsey, *Microwave Remote Sensing of Sea Ice*. Washington, DC: Amer. Geophys. Union, 1992.

[16] F. T. Ulaby, R. K. Moore, and A. K. Fung, *Microwave Remote Sensing, Active and Passive*, vol. 2, *Radar Remote Sensing and Surface Scattering and Emission Theory*, Reading, MA: Addison-Wesley, 1982.

[17] J. P. Hollinger, J. L. Pierce, and G. A. Poe, "SSM/I instrument evaluation," *IEEE Trans. Geosci. Remote Sens.*, vol. 28, no. 5, pp. 781–790, Sep. 1990.

[18] M. Spencer, C. Wu, and D. Long, "Tradeoffs in the design of a spaceborne scanning pencil-beam scatterometer," *IEEE Trans. Geosci. Remote Sens.*, vol. 35, no. 1, pp. 115–126, Jan. 1997.

[19] D. Early and D. Long, "Image reconstruction and enhanced resolution imaging from irregular samples," *IEEE Trans. Geosci. Remote Sens.*, vol. 39, no. 2, pp. 291–302, Feb. 2001.

[20] D. G. Long and D. Daum, "Spatial resolution enhancement of SSM/I data," *IEEE Trans. Geosci. Remote Sens.*, vol. 36, no. 2, pp. 407–417, Mar. 1997.

[21] Scatterometer Climate Record Pathfinder. (2005). [Online]. Available: http://www.scp.byu.edu/

[22] M. R. Drinkwater, D. G. Long, and A. W. Bingham, "Greenland snow accumulation estimates from satellite radar scatterometer data," *J. Geophys. Res.*, vol. 106, no. D24, pp. 33 935–33 950, Dec. 2001.

[23] D. P. Winebrenner, D. G. Long, and B. Holt, "Mapping the progression of melt onset and freeze-up on arctic sea ice using SAR and scatterometry," in *Recent Advances in the Analysis of SAR Data of the Polar Oceans*, C. Tsatsoulis and R. Kwok, Eds. Berlin, Germany: Springer-Verlag, 1998, pp. 129–144.

[24] D. G. Vaughan and C. S. M. Doake, "Recent atmospheric warming and retreat of ice shelves on the Antarctic Peninsula," *Nature*, vol. 379, no. 6563, pp. 328–331, Jan. 1996.

Lukas B. Kunz received the M.S. degree in electrical engineering from Brigham Young University (BYU), Provo, UT, in 2004.

At BYU, he was with the BYU Center for Remote Sensing, focusing on scatterometer applications of microwave remote sensing. He is currently a Radar Design Engineer with emphasis on signal processing algorithms for Raytheon Missile Systems, Tucson, AZ.

David G. Long (S'80–M'82–SM'98) received the Ph.D. degree in electrical engineering from the University of Southern California, Los Angeles, in 1989.

From 1983 to 1990, he was with NASA's Jet Propulsion Laboratory (JPL), where he developed advanced radar remote sensing systems. While at JPL, he was the Project Engineer on the NASA Scatterometer (NSCAT) project, which flew from 1996 to 1997. He also managed the SCANSCAT project, the precursor to SeaWinds, which was launched in 1999 and 2002. He is currently a Professor in the Department of Electrical and Computer Engineering, Brigham Young University (BYU), Provo, UT, where he teaches upper-division and graduate courses in communications, microwave remote sensing, radar, and signal processing, and is the Director of the BYU Center for Remote Sensing. He is the Principle Investigator of several NASA-sponsored research projects in remote sensing. He has authored or coauthored more than 275 publications in signal processing and radar scatterometry. His research interests include microwave remote sensing, radar theory, space-based sensing, estimation theory, signal processing, and mesoscale atmospheric dynamics.

Dr. Long has received the NASA Certificate of Recognition several times. He is an Associate Editor of the IEEE GEOSCIENCE AND REMOTE SENSING LETTERS.